

# Experimental investigation and thermodynamic assessment of the Mg–Zn–Gd system focused on Mg-rich corner

H. Y. Qi · G. X. Huang · H. Bo · G. L. Xu ·  
L. B. Liu · Z. P. Jin

Received: 28 March 2011 / Accepted: 25 August 2011 / Published online: 14 September 2011  
© Springer Science+Business Media, LLC 2011

**Abstract** The phase equilibria in the Mg-rich corner of Mg–Zn–Gd ternary system at 673 K were investigated by means of X-ray diffraction (XRD), scanning electron microscopy (SEM) equipped with energy dispersive X-ray spectroscopy (EDS), and electron probe microanalysis (EPMA). Three ternary phases, X-(Mg<sub>12</sub>ZnGd), W-(Mg<sub>3</sub>Zn<sub>3</sub>Gd<sub>2</sub>) and I-(Mg<sub>3</sub>Zn<sub>6</sub>Gd<sub>1</sub>), have been identified, which are in equilibrium with Mg solid solution. A thermodynamic modeling and optimization of Zn–Gd and Mg–Zn–Gd systems has been carried out for the first time using the CALPHAD method. The sublattice model was used to describe the thermodynamic functions of both solution phases and intermetallic phases presented in these systems. In particular, order/disorder transition between BCC\_B2 and BCC\_A2 has been taken into account, and their Gibbs energies were expressed with identical function. The thermodynamic database was applied to case studies of experimentally observed microstructures and demonstrated that it is a valuable basis for alloy design.

## Introduction

In the past decades, magnesium alloys have attracted increasing attention because of their high strength-to-weight ratio in automotive and aerospace applications

[1, 2]. However, the use of magnesium alloys is currently limited to some extent due to their low mechanical properties at elevated temperatures. Magnesium alloys containing rare-earth elements are found to exhibit higher strength and better creep resistance than other Mg alloys [3, 4]. Gadolinium is often used due to its high solubility in Mg matrix [5]. Addition of a certain amount of Zn can further improve strengthening response of Mg-RE alloys. Nie et al. [6] reported that addition of 1–2 wt% Zn in Mg–6Gd–0.6Zr (wt%) can cause significant enhancement of age-hardening response and the creep strength. Mg–Zn–RE (ZE or EZ series) alloys have been commercialized as heat-resistant alloys [7]. In Mg–Zn–Gd alloys, stable icosahedral quasicrystal phase (I phase) has been identified [8–11]. Quasicrystals have unique properties such as high strength, high hardness, high corrosion resistance, low coefficient of friction and low surface energy, etc. [12]. Yuan et al. [10, 11] reported Mg–Zn–Gd-based alloy strengthened by quasicrystal phase exhibits better creep properties compared to AE42 alloy and higher room temperature mechanical properties close to that of AZ91 alloy. For Mg–Zn–Gd alloys annealed at high temperatures [13–16], a coherent 14H long period stacking ordered structure precipitate formed from the matrix. The alloys, with LPSO structure, performed remarkable high tensile yield strength and high ductility.

Although a number of experimental investigations of microstructure evolution in Mg–Zn–Gd alloys have been reported, phase diagram of Mg–Zn–Gd system has not been established yet. Detailed information about phase equilibria is critical in material design and manufacture. Computational thermodynamics offers an important tool for material design to reduce the experimental effort and costs during new materials development [17]. This work is dedicated to present a thermodynamic description of Mg–Zn–Gd system.

---

H. Y. Qi · G. X. Huang · H. Bo · G. L. Xu ·  
L. B. Liu (✉) · Z. P. Jin  
School of Material Science and Engineering, Central South University, 410083 Changsha, Hunan, People's Republic of China  
e-mail: pdc@mail.csu.edu.cn

L. B. Liu · Z. P. Jin  
Center of Phase Diagram & Materials Design and Manufacture,  
410083 Changsha, Hunan, People's Republic of China

In this paper, (1) experimental investigation into isothermal section at 673 K in Mg-rich corner will be presented and (2) a thermodynamic optimization of Zn–Gd and Mg–Zn–Gd systems will be performed using CALPHAD method based on available experimental data.

## Literature data

### Mg–Zn and Mg–Gd binary systems

Thermodynamic assessment of Mg–Zn system has been performed by Agarwal et al. [18], which is in good agreement with most experimental data on thermodynamic properties and phase boundaries. The optimization of this binary system was improved by Liang et al. [19] using new experimental data in the assessment of Al–Mg–Zn ternary system. Recently, new experimental values of the enthalpies of formation of all the intermediate phases in Mg–Zn system were determined by Berche et al. [20]. The experimental results are in good agreement with the assessed ones [19]. Thus, we can assume that the values assessed by Liang et al. [19] for the Mg–Zn system are reliable. Then they were employed in the present work for higher-order assessment.

Cacciamani et al. [21, 22] and Guo et al. [23] have optimized the Mg–Gd binary system. The thermodynamic parameters of Guo et al. [23] were adopted in the present work because the order–disorder transformation between BCC\_B2 and BCC\_A2 phase was taken into account.

The calculated phase diagrams of Mg–Gd and Mg–Zn systems were shown in Fig. 1.

### Zn–Gd binary system

Massalski et al. [24] showed a schematic Zn–Gd phase diagram based on experimental information summarized in [25]. Liquidus boundaries were mostly unknown, and all known GdZn and GdZn<sub>2</sub> compounds melt congruently. Saccone et al. [26] investigated the whole Zn–Gd phase diagram by means of differential thermal analysis, optical microscopy, scanning electron microscopy, electron probe microanalysis and X-ray diffraction. Eight intermetallic phases were found: GdZn, cubic, cP2-CsCl type, congruent melting at 1020 °C; GdZn<sub>2</sub>, orthorhombic, oI12-CeCu<sub>2</sub> type, congruent melting at 1010 °C; GdZn<sub>3</sub>, orthorhombic, oP16-YZn<sub>3</sub> type, peritectic decomposition at 905 °C; Gd<sub>3</sub>Zn<sub>11</sub>, orthorhombic, oI28-La<sub>3</sub>Al<sub>11</sub> type, peritectic decomposition at 880 °C; Gd<sub>13</sub>Zn<sub>58</sub>, hexagonal, hP142-Gd<sub>13</sub>Zn<sub>58</sub> type, melting at 920 °C; Gd<sub>3</sub>Zn<sub>22</sub>, tetragonal, tI100-Pu<sub>3</sub>Zn<sub>22</sub> type, peritectic decomposition at 910 °C; Gd<sub>2</sub>Zn<sub>17</sub>, high-temperature form, rhombohedral, hR57-Th<sub>2</sub>Zn<sub>17</sub> type and low-temperature form, hexagonal, hP38-Th<sub>2</sub>Ni<sub>17</sub> type, congruent melting at 935 °C; and GdZn<sub>12</sub>, tetragonal, tI26-ThMn<sub>12</sub> type, peritectic

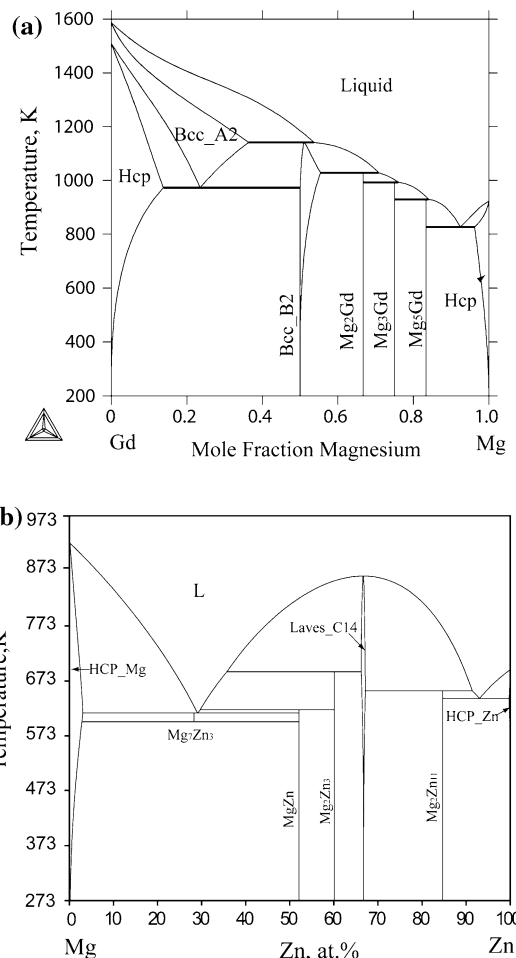


**Fig. 1** Calculated binary phase diagrams of the (a) Mg–Gd and (b) Mg–Zn systems using the thermodynamic data of Guo et al. [19] and Liang et al. [20] respectively

decomposition at 660 °C. Five eutectic reactions occur at 780 °C and 27 at.% Zn ( $\alpha$ Gd) + GdZn) at 945 °C and 59 at.% Zn (GdZn + GdZn<sub>2</sub>), at 875 °C and 77 at.% Zn (GdZn<sub>3</sub> + Gd<sub>3</sub>Zn<sub>11</sub>), at 885 °C and 84 at.% Zn (Gd<sub>13</sub>Zn<sub>58</sub> + Gd<sub>3</sub>Zn<sub>22</sub>) and finally at 400 °C and 99.5 at.% Zn (GdZn<sub>12</sub> + (Zn)). A catalectic equilibrium was found in the Gd-rich end.

No thermodynamic data of the Zn–Gd alloys have been reported; however, the enthalpy of the formation of the intermediate phases of other Zn–RE systems are measured [27, 28]. Because of the similar chemical and physical properties of the rare earths, we can make a comparison with the known thermodynamic properties of Zn with other rare earths. In general, the minima of formation enthalpy generally correspond to the REZn<sub>2</sub> compounds.

### Ternary system

The experimental phase diagram of Mg–Zn–Gd ternary system has not previously been reported, although several ternary compounds have been discovered [8–11, 13–16].

(1) I-(Mg<sub>3</sub>Zn<sub>6</sub>Gd<sub>1</sub>): Liu et al. [10, 11] indicated that the I phase in Mg–Zn–Gd alloys is a face-centered icosahedral quasicrystal with approximately composition of 41.8 at.% Mg, 49.6 at.% Zn and 8.58 at.% Gd.

(2) X-(Mg<sub>12</sub>ZnGd): Yamasaki et al. [13] found that heat treatment at 773 K produces the coherent 14H LPSO structure precipitates from α-Mg supersaturated solid solution. Wu et al. [14, 15] investigated the formation and characterization of the lamellar 14H LPSO structure. The lattice constants of 14H LPSO structure are estimated to be *a* = 0.325 nm, *c* = 3.722 nm, and its composition are established to be Mg-8.10 ± 1.0 at.% Zn-11.05 ± 1.0 at.% Gd.

The microstructure of Mg–10Gd–3Y–1.8Zn–0.5Zr (wt%) alloys with different cooling rates were investigated by Zhang et al. [16]. Two kinds of LPSO structure were observed, including 14H LPSO structure in the grain interior and X phase at the grain boundaries. Lamellar 14H LPSO structure in Mg matrix propagated in the matrix with the decrease of solidification rate. 14H LPSO-structured X phase transformed from eutectic phase when solidification rates are low.

(3) W-(Mg<sub>3</sub>Zn<sub>3</sub>Gd<sub>2</sub>): W phase has a face-centered cubic structure with composition of 31.2 at.% Mg, 43.1 at.% Zn and 25.7 at.% Gd, and the lattice parameter is estimated to be *a* = 0.768 nm by Liu et al. [10, 11]. Padezhnova et al. [29] determined the structure of the W-Mg<sub>3</sub>Zn<sub>3</sub>Y<sub>2</sub> phase by X-ray diffraction. It has a similar structure as AlMnCu<sub>2</sub>-type face-centered cubic (fcc) structure, and its space group is *Fm*  $\bar{3}m$ . As shown from the structural model of the W phase, four Y atoms occupy the 4(a) positions of the AlMnCu<sub>2</sub>-type structure, four Mg atoms the 4(b) positions and eight (Mg + Zn) atoms, with the ratio of 1:3, occupy the 8(c) positions.

In Table 1, crystallographic data of reported ternary Mg–Zn–Gd phases and binary subsystems are summarized.

### Experimental procedure

Mg blocks (99.96 wt% purity), Zn blocks (99.9 wt% purity) and Mg–39.92 wt% Gd master alloy were used as starting materials. Their surfaces were pre-grinded using SiC paper and then were cleaned with 99% ethanol for some minutes in the ultrasonic bath. Thirteen ternary alloys, each with a total weight of approximately 20 g, were prepared in this work. In order to avoid evaporation and oxidation, the samples were sealed in tantalum crucibles by electric arc welding under argon atmosphere. No reactions between the crucibles and the samples were observed. Then, the welded tantalum crucible containing the sample was encapsulated in a quartz tube filled with

**Table 1** Crystallographic data of solid phases in Mg–Gd, Mg–Zn, Zn–Gd and Mg–Zn–Gd systems

Phase	Pearson symbol, space group, structure type	Lattice parameters (nm)		
		<i>a</i> (nm)	<i>b</i> (nm)	<i>c</i> (nm)
(Mg)	hP2, <i>P6</i> <sub>3</sub> / <i>mmc</i> , A3	0.3209		0.5211
(Zn)	hP2, <i>P6</i> <sub>3</sub> / <i>mmc</i> , A3	0.2665		0.4947
(βGd)	cI2, <i>Im</i> $\bar{3}m$ , A2			
(αGd)	hP2, <i>P6</i> <sub>3</sub> / <i>mmc</i> , A3	0.3629		0.5760
GdMg <sub>5</sub>	cF*, <i>F</i> $\bar{4}3m$			
GdMg <sub>3</sub>	cF16, <i>Fm</i> $\bar{3}m$ , D0 <sub>3</sub>	0.7321		
GdMg <sub>2</sub>	cF24, <i>Fd</i> $\bar{3}m$ , C15	0.8575		
GdMg	cP2, <i>Pm</i> $\bar{3}m$ , B2	0.3812		
GdZn	cP2, <i>Pm</i> $\bar{3}m$ , B2	0.3617		
GdZn <sub>2</sub>	oI12, <i>Imma</i>	0.4446	0.7174	0.7585
GdZn <sub>3</sub>	oP16, <i>Pnma</i>	0.6694	0.4418	1.0161
Gd <sub>3</sub> Zn <sub>11</sub>	oI28, <i>Immm</i>	0.4425	1.3082	0.8800
Gd <sub>13</sub> Zn <sub>58</sub>	hP142, <i>P6</i> <sub>3</sub> / <i>mc</i>	1.434		1.406
Gd <sub>3</sub> Zn <sub>22</sub>	tI100, <i>I4</i> <sub>1</sub> / <i>amd</i>	0.8900		2.1359
βGd <sub>2</sub> Zn <sub>17</sub> (HT)	hR57, <i>R</i> $\bar{3}m$	0.8992		1.3163
αGd <sub>2</sub> Zn <sub>17</sub> (LT)	hP38, <i>P6</i> <sub>3</sub> / <i>mmc</i>	0.8980		0.8770
GdZn <sub>12</sub>	tI26, <i>I4</i> / <i>mmm</i> , D2 <sub>b</sub>	0.8898		0.5210
Mg <sub>51</sub> Zn <sub>20</sub>	oI158, <i>Immm</i>	1.4083	1.4486	1.4025
MgZn		0.533	0.923	1.716
Mg <sub>2</sub> Zn <sub>3</sub>	mC110, <i>B2</i> / <i>m</i>	2.596	1.428	0.524
MgZn <sub>2</sub>	hP12, <i>P6</i> <sub>3</sub> / <i>mmc</i> , C14	0.5223		0.8566
Mg <sub>2</sub> Zn <sub>11</sub>	cP39, <i>Pm</i> $\bar{3}$ , D8 <sub>c</sub>	0.8552		
X-Mg <sub>12</sub> ZnGd	?	0.325		3.722
W-Mg <sub>3</sub> Zn <sub>3</sub> Gd <sub>2</sub>		0.768		
I-Mg <sub>3</sub> Zn <sub>6</sub> Gd <sub>1</sub>				

pure argon to avoid the reaction of tantalum crucible in air environment. After melted at 1173 K for 2 h, the samples were quenched in water. During melting, the capsules were turned up and down every 30 min for the alloy composition homogenization. All the quenched alloys were annealed at 673 K for 720 h and then water-quenched.

Phase identification was carried out by X-ray diffraction (XRD) (Dmax-2500VBX) with Cu Kα diffraction, at 40 kV and 250 mA. The microstructure of each alloy was examined using scanning electron microscopy (SEM) (FEI Quanta 200) equipped with energy dispersive X-ray spectroscopy (EDS) (EDS GENESIS 60S). At least three valid EDS point analyzes were made for each phase in order to guarantee a good analysis of their compositions. The samples were ground and polished under alcohol to avoid reaction with water. To acquire more accurate data, the composition of each phase was studied by electron probe microanalysis (EPMA) (JXA-8800R, JEOL, Japan) using a 20 kV voltage and 20 nA current. The high-pure Mg, Zn

and Gd were served as standards to revise the characteristic radiations.

### Thermodynamic models

There are solution phases, stoichiometric intermetallic compounds and intermetallic compounds with noticeable solubility ranges in Mg–Zn–Gd system. In order to maintain consistency with other thermodynamic assessment, the Gibbs energies of the pure elements, referred to the enthalpy of each element in its so-called standard element reference (SER) state (the stable state at  $10^5$  Pa and 298.15 K), were taken from the Science Group Thermodata Europe (SGTE) Pure Elements Database [30].

#### Solution phases

The Gibbs energies of solution phases, liquid, BCC\_A2, FCC\_A1, HCP\_A3 and HCP\_Zn are described with the substitutional solution model based on random mixing of the metal atoms as follows:

$$G_m^\Phi = \sum_{i=\text{Gd,Mg,Zn}} x_i^0 G_i^\Phi + RT \sum_{i=\text{Gd,Mg,Zn}} x_i \ln x_i + {}^E G_m^\Phi + {}^{\text{mg}} G_m^\Phi \quad (1)$$

where  ${}^0 G_i^\Phi$  is the molar Gibbs energy of pure element  $i$  ( $i = \text{Gd, Mg, Zn}$ ) with structure  $\Phi$ ;  $R$  is gas constant;  $T$  is the temperature in K;  $x_i$  is mole fractions of component  $i$  and  ${}^E G_m^\Phi$  is the excess Gibbs energy formulated with the Redlich–Kister polynomial [31] as

$$\begin{aligned} {}^E G_m^\Phi = & x_{\text{Gd}} x_{\text{Mg}} \sum_i {}^i L_{\text{Gd,Mg}}^\Phi (x_{\text{Gd}} - x_{\text{Mg}})^i \\ & + x_{\text{Mg}} x_{\text{Zn}} \sum_i {}^i L_{\text{Mg,Zn}}^\Phi (x_{\text{Mg}} - x_{\text{Zn}})^i \\ & + x_{\text{Gd}} x_{\text{Zn}} \sum_i {}^i L_{\text{Gd,Zn}}^\Phi (x_{\text{Gd}} - x_{\text{Zn}})^i \\ & + x_{\text{Gd}} x_{\text{Mg}} x_{\text{Zn}} {}^i L_{\text{Gd,Mg,Zn}}^\Phi \end{aligned} \quad (2)$$

where  ${}^i L_{\text{Gd,Mg}}^\Phi$ ,  ${}^i L_{\text{Mg,Zn}}^\Phi$  and  ${}^i L_{\text{Gd,Zn}}^\Phi$  are the interaction parameters between elements Gd and Mg, Mg and Zn, and Gd and Zn, respectively;  ${}^i L_{\text{Gd,Mg,Zn}}^\Phi$  is the ternary interaction parameter;  ${}^i L_{\text{Gd,Zn}}^\Phi$  and  ${}^i L_{\text{Gd,Mg,Zn}}^\Phi$  are to be evaluated in the present work. The general form of the interaction parameters is

$$L^\Phi = a + bT + cT \ln T + dT^2 + eT^3 + fT^{-1} \quad (3)$$

In most cases, only the first one or two terms are used according to the temperature dependence on the experimental data.  ${}^{\text{mg}} G_m^\Phi$  is the magnetic contribution to the Gibbs energy. Due to a lack of experimental data about

magnetism, the interaction parameters  ${}^{\text{mg}} G_m^\Phi$  were not optimized in the present work.

#### Ordered solid solutions

The compounds MgGd and GdZn have the same BCC\_B2 structure and probably form a cP2-CsCl-type solution in the Mg–Zn–Gd ternary system. In order to indicate their structural relationship between ordered BCC\_B2 and disordered BCC\_A2, the two phases are modeled using a single function based on the two-sublattices (Gd,Mg,Zn)<sub>0.5</sub>(Gd,Mg,Zn)<sub>0.5</sub> with the following form [32]:

$$G_m = G_m^{\text{dis}}(x_i) + G_m^{\text{ord}}(y_i^{\text{I}}, y_i^{\text{II}}) - G_m^{\text{ord}}(x_i, x_i) \quad (4)$$

where  $x_i$  represents the mole fraction of constituent  $i$ , and  $y_i^{\text{I}}$  and  $y_i^{\text{II}}$  are the site fractions, i.e., the mole fractions in the first and second sublattices, respectively. The first term,  $G_m^{\text{dis}}(x_i)$ , represents the Gibbs energy of the disordered phase BCC\_A2, which is expressed by Eq. 1. The second term,  $G_m^{\text{ord}}(y_i^{\text{I}}, y_i^{\text{II}})$ , is the Gibbs energy of the ordered phase BCC\_B2 as described by the sublattice model and contains implicitly a contribution of the disordered state. It is expressed as follows:

$$\begin{aligned} G_m^{\text{ord}}(y_i^{\text{I}}, y_i^{\text{II}}) = & \sum_i \sum_j y_i^{\text{I}} y_j^{\text{II}0} G_{ij} \\ & + 0.5RT \sum_i (y_i^{\text{I}} \ln y_i^{\text{I}} + y_i^{\text{II}} \ln y_i^{\text{II}}) \\ & + y_A^{\text{I}} y_B^{\text{I}} y_A^{\text{II}} \sum_{v=0,1,\dots} {}^v L_{\text{A,B:A}} (y_A - y_B)^v \\ & + y_A^{\text{I}} y_B^{\text{I}} y_B^{\text{II}} \sum_{v=0,1,\dots} {}^v L_{\text{A,B:B}} (y_A - y_B)^v \\ & + y_A^{\text{I}} y_A^{\text{II}} y_B^{\text{II}} \sum_{v=0,1,\dots} {}^v L_{\text{A:A,B}} (y_A - y_B)^v \\ & + y_B^{\text{I}} y_A^{\text{II}} y_B^{\text{II}} \sum_{v=0,1,\dots} {}^v L_{\text{B:A,B}} (y_A - y_B)^v \end{aligned} \quad (5)$$

The parameters  ${}^v L$  have the form shown in Eq. 3. Due to the crystallographical symmetry, the following relations are introduced in [33]:

$${}^0 G_{j:i} = {}^0 G_{i:j} \quad {}^v L_{i:i,j} = {}^v L_{i,j:i} \quad (6)$$

The last term,  $G_m^{\text{ord}}(x_i, x_i)$ , represents the energy contribution of the disordered state to the ordered phase. The last two terms cancel each other when the site fractions are equal, thus corresponding to a disordered phase. Hence, the parameters of both ordered and disordered phases can be evaluated independently.

#### Binary intermetallic phases

Because of the negligible solid solubilities for the third element, all the binary intermetallic compounds in Zn–Gd system except GdZn are treated as stoichiometric phases

**Table 2** Constituent phases and compositions of Mg–Zn–Gd alloys annealed at 673 K for 720 h

Alloys	Nominal composition (at.%)	Phases identified by XRD	Phases distinguished by BSE and EPMA	Phase composition (at.%)–EPMA data		
				Mg	Gd	Zn
1	Mg94.5Zn0.5Gd5	(Mg)	(Mg)	98.00	1.83	0.17
		X	X	89.82	6.09	4.09
			Mg <sub>5</sub> Gd	79.42	17.65	2.93
2	Mg97Zn2Gd1	(Mg)	(Mg)	99.07	0.67	0.25
		W	W	42.50	22.32	35.17
		X	X	89.69	5.67	4.64
3	Mg96Zn2Gd2	(Mg)	(Mg)	97.90	0.11	1.99
		W	W	32.65	22.83	44.52
		X	X	92.13	2.31	5.56
4	Mg95.5Zn4Gd0.5	(Mg)	(Mg)	98.04	0.04	1.92
		W	W	32.52	19.76	47.72
		X	X	93.71	1.54	4.75
5	Mg88.6Zn2.0Gd9.4	(Mg)	(Mg)	99.20	0.58	0.22
		W	W	37.52	23.85	38.63
		X	X	90.27	5.54	4.19
6	Mg95Zn4Gd1	(Mg)	(Mg)	97.75	0.02	2.23
		I	I	39.15	7.17	53.68
		W	W	26.20	25.11	48.68
7	Mg98Zn1Gd1	(Mg)	(Mg)	97.76	0.01	2.22
		W	W	26.05	24.89	49.06
		I	I	37.82	8.29	53.89
8	Mg97Zn1Gd2	(Mg)	(Mg)	97.77	0.02	2.22
		W	W	25.52	25.31	49.17
		I	I	39.09	7.73	53.17
9	Mg89.6Zn7.6Gd2.8	(Mg)	(Mg)	99.45	0.10	0.46
		W	W	43.01	19.51	37.47
10	Mg88.3Zn10Gd1.7	(Mg)	(Mg)	97.95	0.03	2.02
		W	W	27.21	24.49	48.30
11	Mg88Zn10Gd2	(Mg)	(Mg)	99.20	0.56	0.23
		X	X	90.85	5.21	3.94
12	Mg87.4Zn11.6Gd1.0	(Mg)	(Mg)	98.87	0.98	0.15
		X	X	90.37	5.66	3.97
13	Mg94Zn5Gd1.0	(Mg)	(Mg)	97.62	0.01	2.37
			Mg <sub>7</sub> Zn <sub>3</sub>	69.55	0.08	30.37
		I	I	60.52	5.57	33.91

Zn<sub>p</sub>Gd<sub>q</sub>. According to the Neumann–Kopp rule, the Gibbs energy of Zn<sub>p</sub>Gd<sub>q</sub> can be formulated as:

$$G_{Zn_pGd_q} = \frac{p}{p+q} {}^0G_{Zn}^{HCP-Zn} + \frac{q}{p+q} {}^0G_{Gd}^{HCP-A3} + A + BT \quad (7)$$

where A and B are the adjustable parameters to be optimized in this work.

The Mg<sub>5</sub>Gd with a homogeneity range was modeled as (Mg,Zn)<sub>5</sub>Gd in the Mg–Zn–Gd system. According to the general sublattice model [34], the Gibbs energy is expressed as:

$$G_{(Mg,Zn)_5Gd} = y'_{Mg} G_{Mg:Gd}^{(Mg,Zn)_5Gd} + y'_{Zn} G_{Zn:Gd}^{(Mg,Zn)_5Gd} + \frac{5}{6} RT \left( y'_{Mg} \ln y'_{Mg} + y'_{Zn} \ln y'_{Zn} \right) + y'_{Mg} y'_{Zn} \left( \sum_i^i L_{Mg,Zn:Gd}^{(Mg,Zn)_5Gd} \left( y'_{Mg} - y'_{Zn} \right)^i \right) \quad (8)$$

where  $G_{Mg:Gd}^{(Mg,Zn)_5Gd}$  has the same value as  $G_{Mg_5Gd}^{Mg_5Gd}$ , and  $G_{Zn:Gd}^{(Mg,Zn)_5Gd}$  represents Gibbs energy of the hypothetical Zn<sub>5</sub>Gd, which is formalized as

$$G_{Zn:Gd}^{(Mg,Zn)_5Gd} = \frac{5}{6} G_{Zn}^{HCP-Zn} + \frac{1}{6} G_{Gd}^{HCP-A3} + C + DT \quad (9)$$

where  $C$  and  $D$  are the parameters to be optimized in this work.

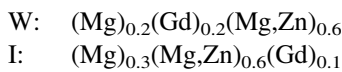
### Ternary intermetallic compounds

In the Mg–Zn–Gd ternary system, stoichiometric intermetallic phase, X-Mg<sub>12</sub>ZnGd, is modeled as Mg<sub>x</sub>Zn<sub>y</sub>Gd<sub>z</sub>, and its Gibbs energy expression is written as:

$$G_{Mg_xZn_yGd_z} = \frac{x}{x+y+z} G_{Mg}^{HCP-A3} + \frac{y}{x+y+z} G_{Zn}^{HCP-Zn} + \frac{z}{x+y+z} G_{Gd}^{HCP-A3} + E + FT \quad (10)$$

where  $E$  and  $F$  are the parameters to be optimized.

W-Mg<sub>3</sub>Zn<sub>3</sub>Gd<sub>2</sub> and I-Mg<sub>3</sub>Zn<sub>6</sub>Gd<sub>1</sub> in the Mg–Zn–Gd system has a homogeneity range and are treated as the following formula by a three-sublattice model [35]:



The Gibbs energies for a general three-sublattice model (Mg,Zn)<sub>x</sub>(Mg,Zn)<sub>y</sub>(Gd)<sub>z</sub> are expressed as follows::

$$G_m^{(Mg,Zn)_x(Mg,Zn)_yGd_z} = y'_Mg y''_Mg G_{Mg:Mg:Gd}^{(Mg,Zn)_x(Mg,Zn)_yGd_z} + y'_Mg y''_Zn G_{Mg:Zn:Gd}^{(Mg,Zn)_x(Mg,Zn)_yGd_z} + y'_Zn y''_Mg G_{Zn:Mg:Gd}^{(Mg,Zn)_x(Mg,Zn)_yGd_z} + y'_Zn y''_Zn G_{Zn:Zn:Gd}^{(Mg,Zn)_x(Mg,Zn)_yGd_z} + xRT (y'_Mg \ln y'_Mg + y'_Zn \ln y'_Zn) + yRT (y''_Mg \ln y''_Mg + y''_Zn \ln y''_Zn) + y'_Mg y''_Mg y''_Zn \left[ \sum_i L_{Mg:Mg:Zn:Gd}^{(Mg,Zn)_x(Mg,Zn)_yGd_z} (y''_Mg - y''_Zn)^i \right] + y'_Zn y''_Mg y''_Zn \left[ \sum_i L_{Zn:Mg:Zn:Gd}^{(Mg,Zn)_x(Mg,Zn)_yGd_z} (y''_Mg - y''_Zn)^i \right] + y'_Mg y'_Zn y''_Mg \left[ \sum_i L_{Mg:Zn:Mg:Gd}^{(Mg,Zn)_x(Mg,Zn)_yGd_z} (y'_Mg - y'_Zn)^i \right] + y'_Mg y'_Zn y''_Zn \left[ \sum_i L_{Mg,Zn:Zn:Gd}^{(Mg,Zn)_x(Mg,Zn)_yGd_z} (y'_Mg - y'_Zn)^i \right] + y'_Mg y'_Zn y''_Mg y''_Zn \left[ \sum_i L_{Mg,Zn:Mg,Zn:Gd}^{(Mg,Zn)_x(Mg,Zn)_yGd_z} (y'_Mg - y'_Zn)^i (y''_Mg - y''_Zn)^i \right] \quad (11)$$

## Results and discussion

### Experimental results

The constituent phases and their compositions in the selected alloys are listed in Table 2. Three ternary phases, X-(Mg<sub>12</sub>ZnGd), W-(Mg<sub>3</sub>Zn<sub>3</sub>Gd<sub>2</sub>) and I-(Mg<sub>3</sub>Zn<sub>6</sub>Gd<sub>1</sub>), are in direct equilibrium with the Mg solid solution. The existence of a ternary solid solution of Mg<sub>5</sub>Gd was confirmed. The determined isothermal section of Mg–Zn–Gd ternary system at 673 K in the Mg-rich region was shown in Fig. 2. The triangles drawn in as dotted lines indicate three-phase equilibria, and the thick dotted lines are the measured tie-lines.

According to the EPMA results, the composition of X-Mg<sub>12</sub>ZnGd is about 88.1–89.8 at.% Mg, 3.9–4.6 at.% Zn and 5.5–6.1 at.% Gd. The measured composition is very close to the stoichiometric composition of Mg<sub>12</sub>ZnGd reported previously [13, 15].

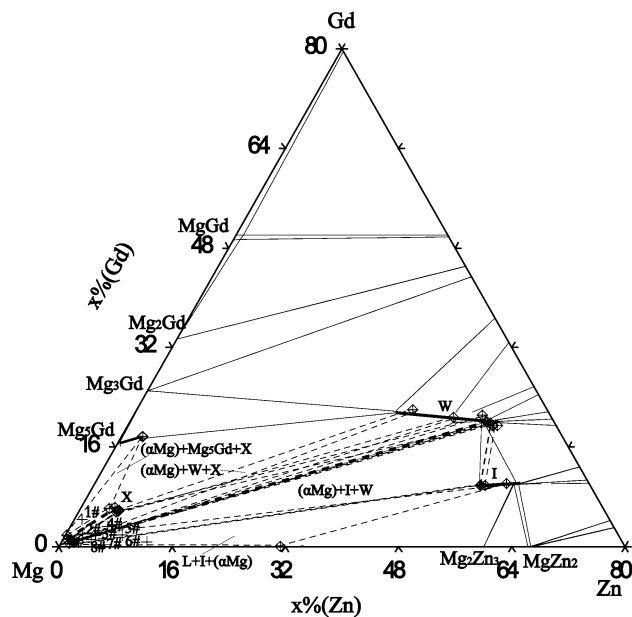


**Fig. 2** The partial isothermal section in the Mg-rich corner of the Mg–Zn–Gd system at 673 K. The symbol (+) represents the investigated sample compositions. The *thick dotted lines* are the measured tie-lines. The *triangles* drawn in as *dotted lines* indicate three-phase equilibria. The symbol (◆) denotes the phase compositions

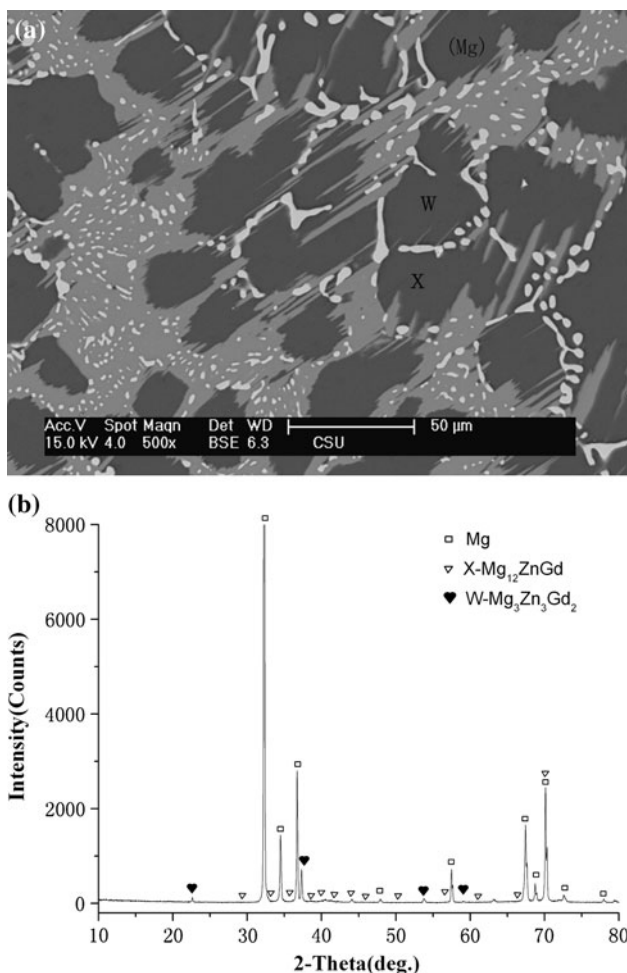


**Fig. 3** The BSE image (a) and X-ray diffraction profile (b) of alloy 2#

The composition of W phase determined in this work is Mg: 45–50 at.%, Zn: 30–35 at.%, Gd: 20 at.%, which is in good agreement with the experimental results Mg<sub>3</sub>Zn<sub>3</sub>Gd<sub>2</sub> (face-centered cubic structure) reported by Liu et al. [10, 11]. I-Mg<sub>3</sub>Zn<sub>6</sub>Gd<sub>1</sub> phase was considered as a Frank–Kasper type with a composition of Mg<sub>42</sub>Zn<sub>50</sub>Gd<sub>8</sub> (at.%) by Tsai et al. [8]. The consistent results have been obtained in this work, Mg: 38 ± 1 at.%, Zn: 54 ± 1 at.%, Gd: 8 ± 1 at.%. Within the investigated composition ranges, three three-phase regions (αMg + X-Mg<sub>12</sub>ZnGd + Mg<sub>5</sub>Gd, αMg + X-Mg<sub>12</sub>ZnGd + W-Mg<sub>3</sub>Zn<sub>3</sub>Gd<sub>2</sub>, αMg + W-Mg<sub>3</sub>Zn<sub>3</sub>Gd<sub>2</sub> + I-Mg<sub>3</sub>Zn<sub>6</sub>Gd<sub>1</sub>) and two two-phase regions (αMg + X-Mg<sub>12</sub>ZnGd, αMg + W-Mg<sub>3</sub>Zn<sub>3</sub>Gd<sub>2</sub>) are determined at 673 K in this work. The SEM micrographs and XRD diffraction profile of alloy 2 are shown in Fig. 3a, b. As is shown in Fig. 3b, the alloy 2 consists of three phases: (αMg), W-Mg<sub>3</sub>Zn<sub>3</sub>Gd<sub>2</sub> and X-Mg<sub>12</sub>ZnGd. Based on the EPMA results, it can be concluded that the dark phase is (αMg), the gray phase is X-Mg<sub>12</sub>ZnGd and the bright phase is W-Mg<sub>3</sub>Zn<sub>3</sub>Gd<sub>2</sub>. The BSE image and X-ray diffraction profile of alloy 6, shown in Fig. 4a, b, consists of

three phases (αMg), W-Mg<sub>3</sub>Zn<sub>3</sub>Gd<sub>2</sub> and I-Mg<sub>3</sub>Zn<sub>6</sub>Gd<sub>1</sub>. Based on the EPMA data, the dark phase is (αMg), the white block phase is W-Mg<sub>3</sub>Zn<sub>3</sub>Gd<sub>2</sub> and the eutectic structure is I-Mg<sub>3</sub>Zn<sub>6</sub>Gd<sub>1</sub> phase. In the image of alloys 13, shown in Fig. 5a, liquid phase exists. Based on the EPMA data, the dark phase is (αMg), the lamellar eutectic phases are I phase surrounding the inner region of Mg<sub>7</sub>Zn<sub>3</sub> phase. The alloy of interest is in the (L + I + (αMg)) equilibrium region, Mg<sub>7</sub>Zn<sub>3</sub> phase forms by the binary peritectic reaction L + (αMg) → Mg<sub>7</sub>Zn<sub>3</sub>.

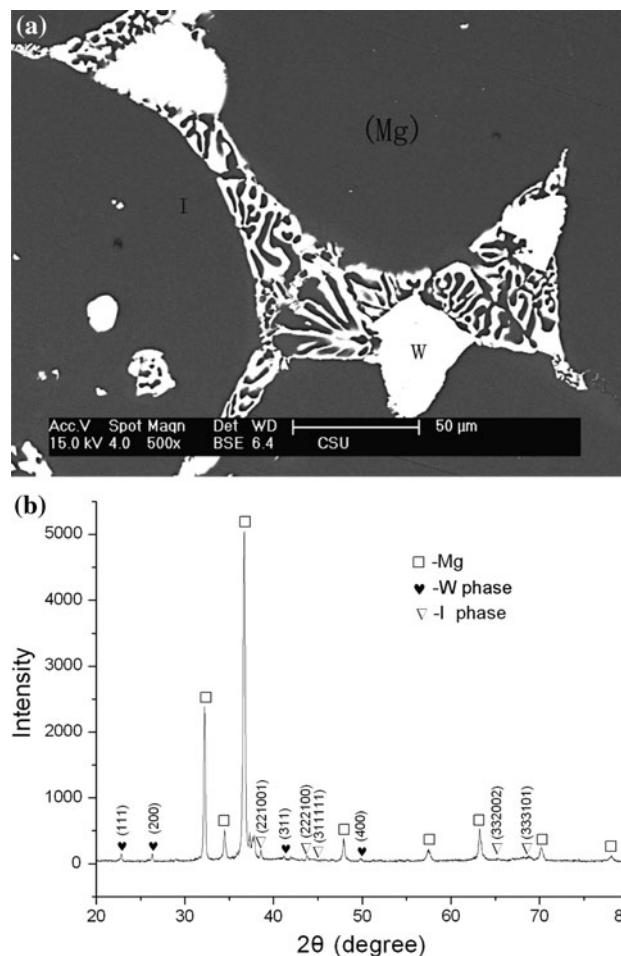


**Fig. 4** The BSE image (a) and X-ray diffraction profile (b) of alloy 6#

three phases (αMg), W-Mg<sub>3</sub>Zn<sub>3</sub>Gd<sub>2</sub> and I-Mg<sub>3</sub>Zn<sub>6</sub>Gd<sub>1</sub>. Based on the EPMA data, the dark phase is (αMg), the white block phase is W-Mg<sub>3</sub>Zn<sub>3</sub>Gd<sub>2</sub> and the eutectic structure is I-Mg<sub>3</sub>Zn<sub>6</sub>Gd<sub>1</sub> phase. In the image of alloys 13, shown in Fig. 5a, liquid phase exists. Based on the EPMA data, the dark phase is (αMg), the lamellar eutectic phases are I phase surrounding the inner region of Mg<sub>7</sub>Zn<sub>3</sub> phase. The alloy of interest is in the (L + I + (αMg)) equilibrium region, Mg<sub>7</sub>Zn<sub>3</sub> phase forms by the binary peritectic reaction L + (αMg) → Mg<sub>7</sub>Zn<sub>3</sub>.

### Thermodynamic modeling

On the basis of lattice stabilities taken from the PURE database [30], the optimization of the Zn–Gd and Mg–Zn–Gd systems is carried out using the PARROT module in the Thermo-Calc software package developed by Sundman et al. [36] based on the experimental data.

Pandat software [37] was used to check the database. All the parameters obtained in present work are listed in Table 3.

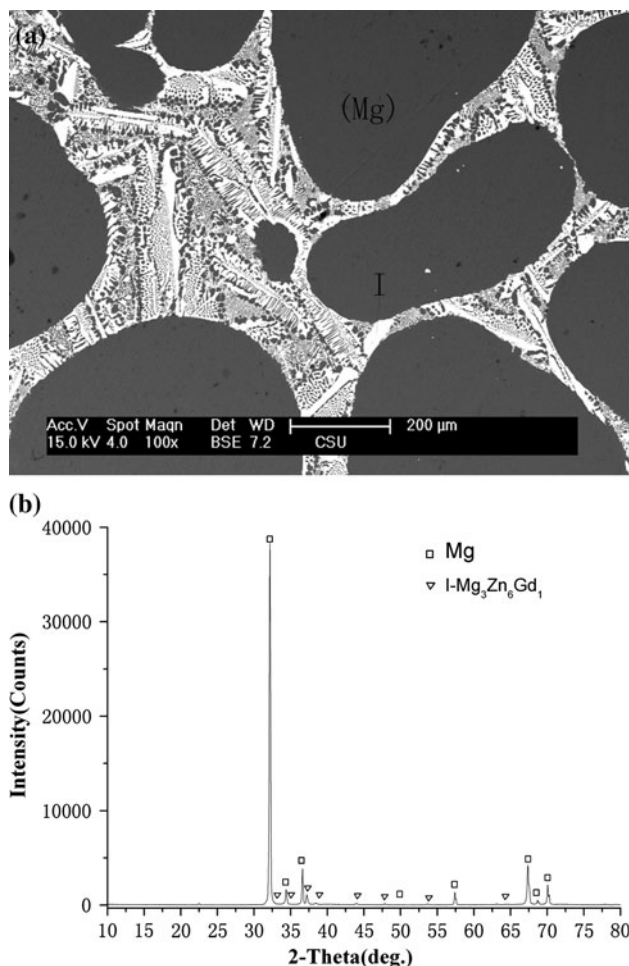


**Fig. 5** The BSE image (a) and X-ray diffraction profile (b) of alloy 13#

Of the three constituent binary systems, the Mg–Gd [23] and Mg–Zn [19] systems have been thermodynamically optimized previously and the parameters are adopted in the present work. Due to the lack of thermodynamic data, no attempt has been made to thermodynamically model the Zn–Gd binary system previously. In this work, all the intermetallic phases in the Zn–Gd system are treated as stoichiometric ones except the ZnGd (BCC\_B2) phase. The calculated phase diagram of the Zn–Gd system compared with the experimental data [26] is shown in Fig. 6. The calculated invariant reactions, shown in Table 4, agree very well with the experimental data. The calculated minima of formation enthalpy correspond to the GdZn<sub>2</sub> phase, which is consistent with the experimental results [27, 28]. The optimized thermodynamic data for Zn–Gd system is satisfactory and can be used for modeling the higher-order system.

All ternary phases in the Mg–Zn–Gd system, the X, W and I phases, are treated with the three-sublattice model on the basis of available crystallographic information. The X phase is treated as stoichiometric one; for W and I phases, mixing between sublattices of Mg and Zn are considered. Based on the experimental results of phase compositions and available crystallographic data, W and I phases are treated as (Mg)<sub>0.2</sub>(Gd)<sub>0.2</sub>(Mg,Zn)<sub>0.6</sub> and (Mg)<sub>0.3</sub>(Gd)<sub>0.1</sub>(Mg,Zn)<sub>0.6</sub>. The calculated isothermal section at 673 K of Mg–Zn–Gd system is shown in Fig. 7a, b. Compared with the experimental isothermal section (Fig. 2), the calculated phase relationships in Mg-rich corner are consistent with the experimental data. Figure 8a, b are the calculated

**Table 3** Thermodynamic parameters of Mg–Zn–Gd system reported in the literatures and optimized in the present work

Phase	Thermodynamic parameters	Ref.
Liquid model: (Gd,Mg,Zn)	${}^0L_{\text{Gd,Mg}}^{\text{Liq}} = -36681.3 + 16.2T$	[23]
	${}^1L_{\text{Gd,Mg}}^{\text{Liq}} = +34233.8 - 10.8T$	[23]
	${}^2L_{\text{Gd,Mg}}^{\text{Liq}} = -7352.9$	[23]
	${}^0L_{\text{Mg,Zn}}^{\text{Liq}} = -77729.2 + 680.5T - 95T \ln(T) + 0.04T^2$	[19]
	${}^1L_{\text{Mg,Zn}}^{\text{Liq}} = +3674.7 + 0.6T$	[19]
	${}^2L_{\text{Mg,Zn}}^{\text{Liq}} = -1588.2$	[19]
	${}^0L_{\text{Gd,Zn}}^{\text{Liq}} = -128000 + 4.2T$	This work
	${}^1L_{\text{Gd,Zn}}^{\text{Liq}} = +56000$	This work
	${}^1L_{\text{Gd,Mg,Zn}}^{\text{Liq}} = -25000$	This work
	BCC_A2 model: (Gd,Mg,Zn) This is the disordered part of BCC_B2	${}^0L_{\text{Gd,Mg}}^{\text{BCC\_A2}} = -45347.5 + 25.5T$
${}^1L_{\text{Gd,Mg}}^{\text{BCC\_A2}} = +10195 + 1.3T$		[23]
${}^2L_{\text{Gd,Mg}}^{\text{BCC\_A2}} = +3267.1 - 3.5T$		[23]
${}^0L_{\text{Gd,Zn}}^{\text{BCC\_A2}} = -50000$		This work

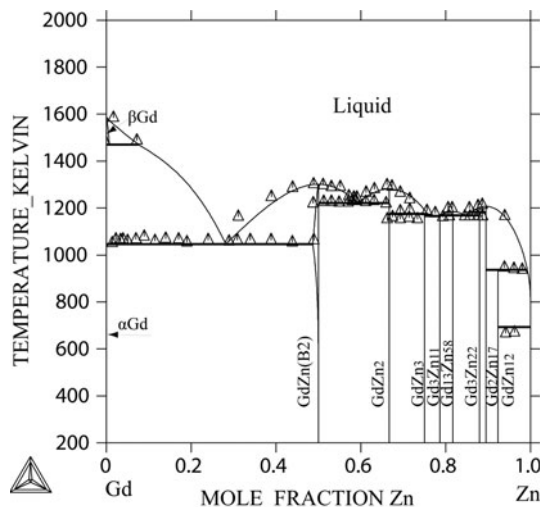


**Table 3** continued

Phase	Thermodynamic parameters	Ref.
BCC_B2 model: (Gd,Mg,Zn) <sub>0.5</sub> (Gd,Mg,Zn) <sub>0.5</sub>	${}^0L_{\text{Gd:Mg}}^{\text{BCC\_B2}} = {}^0L_{\text{Mg:Gd}}^{\text{BCC\_B2}} = -28695.4 + 6.2T$	[23]
	${}^0L_{\text{Gd,Mg:Gd}}^{\text{BCC\_B2}} = {}^0L_{\text{Gd:Gd,Mg}}^{\text{BCC\_B2}} = -15446.6$	[23]
	${}^1L_{\text{Gd,Mg:Gd}}^{\text{BCC\_B2}} = {}^1L_{\text{Gd:Gd,Mg}}^{\text{BCC\_B2}} = -16247.3$	[23]
	${}^0L_{\text{Zn:Gd}}^{\text{BCC\_B2}} = {}^0L_{\text{Gd:Zn}}^{\text{BCC\_B2}} = -53892.4 + 10.6T$	This work
	${}^0L_{\text{Gd,Zn:Zn}}^{\text{BCC\_B2}} = {}^0L_{\text{Zn:Gd,Zn}}^{\text{BCC\_B2}} = +31000$	This work
	${}^1L_{\text{Gd,Zn:Zn}}^{\text{BCC\_B2}} = {}^1L_{\text{Zn:Gd,Zn}}^{\text{BCC\_B2}} = -25000$	This work
	${}^0L_{\text{Gd:Mg,Zn}}^{\text{BCC\_B2}} = {}^0L_{\text{Mg,Zn:Gd}}^{\text{BCC\_B2}} = -12000$	This work
FCC_A1 model: (Gd,Mg,Zn)	${}^0L_{\text{Mg,Zn}}^{\text{FCC}} = -3056.82 + 5.63801T$	[19]
	${}^1L_{\text{Mg,Zn}}^{\text{FCC}} = -3127.26 + 5.65563T$	[19]
	${}^0G_{\text{Gd,Zn}}^{\text{FCC\_A1}} = -67700 + 4T$	This work
	${}^1G_{\text{Gd,Zn}}^{\text{FCC\_A1}} = +27000$	This work
HCP_A3 model: (Gd,Mg,Zn) <sub>1</sub> (Va) <sub>0.5</sub>	${}^0L_{\text{Zn}}^{\text{HCP\_A3}} - {}^0L_{\text{Zn}}^{\text{HCP\_Zn}} = +2969.82 - 1.56968T$	[30]
	${}^0L_{\text{Gd,Mg}}^{\text{HCP\_A3}} = -33346.6 + 19.3T$	[23]
	${}^1L_{\text{Gd,Mg}}^{\text{HCP\_A3}} = +13854$	[23]
	${}^0L_{\text{Mg,Zn}}^{\text{HCP\_A3}} = -3056.8 + 5.6T$	[19]
	${}^1L_{\text{Mg,Zn}}^{\text{HCP\_A3}} = -3127.3 + 5.7T$	[19]
HCP_Zn model: (Gd,Mg,Zn) <sub>1</sub> (Va) <sub>0.5</sub>	${}^0L_{\text{Mg}}^{\text{HCP\_Zn}} - {}^0L_{\text{Mg}}^{\text{HCP\_A3}} = +100$	[30]
	${}^0L_{\text{Mg,Zn}}^{\text{HCP\_Zn}} = -3056.8 + 5.6T$	[19]
	${}^1L_{\text{Mg,Zn}}^{\text{HCP\_Zn}} = -3127.3 + 5.7T$	[19]
Mg <sub>2</sub> Gd model: (Mg) <sub>0.667</sub> (Gd) <sub>0.333</sub>	$G_{\text{Mg:Gd}}^{\text{Mg}_2\text{Gd}} - 0.667{}^0G_{\text{Mg}}^{\text{HCP\_A3}} - 0.333{}^0G_{\text{Gd}}^{\text{HCP\_A3}} = -16925.7 + 5.7T$	[23]
Mg <sub>3</sub> Gd model: (Mg) <sub>0.75</sub> (Gd) <sub>0.25</sub>	$G_{\text{Mg:Gd}}^{\text{Mg}_3\text{Gd}} - 0.75{}^0G_{\text{Mg}}^{\text{HCP\_A3}} - 0.25{}^0G_{\text{Gd}}^{\text{HCP\_A3}} = -13572.45 + 3.25T$	[23]
Mg <sub>5</sub> Gd model: (Mg,Zn) <sub>0.833</sub> (Gd) <sub>0.167</sub>	$G_{\text{Mg:Gd}}^{\text{Mg}_5\text{Gd}} - 0.833{}^0G_{\text{Mg}}^{\text{HCP\_A3}} - 0.167{}^0G_{\text{Gd}}^{\text{HCP\_A3}} = -10086.9 + 1.883T$	[23]
	$G_{\text{Zn:Gd}}^{\text{Mg}_5\text{Gd}} - 0.833{}^0G_{\text{Zn}}^{\text{HCP\_Zn}} - 0.167{}^0G_{\text{Gd}}^{\text{HCP\_A3}} = -130521.6$	This work
Laves_C14 model: (Gd,Mg,Zn) <sub>0.667</sub> (Gd,Mg,Zn) <sub>0.333</sub>	$G_{\text{Mg:Mg}}^{\text{C14}} - {}^0G_{\text{Mg}}^{\text{HCP\_A3}} = +5000$	[19]
	$G_{\text{Zn:Zn}}^{\text{C14}} - {}^0G_{\text{Zn}}^{\text{HCP\_Zn}} = +5000$	[19]
	$G_{\text{Zn:Mg}}^{\text{C14}} - 0.667{}^0G_{\text{Zn}}^{\text{HCP\_Zn}} - 0.333{}^0G_{\text{Mg}}^{\text{HCP\_A3}} = -11785.15 + 2.94629T$	[19]
	$G_{\text{Mg:Zn}}^{\text{C14}} - 0.667{}^0G_{\text{Mg}}^{\text{HCP\_A3}} - 0.333{}^0G_{\text{Zn}}^{\text{HCP\_Zn}} = +21785.15 - 2.94629T$	[19]
	$G_{\text{Mg,Zn:Mg}}^{\text{C14}} = G_{\text{Mg,Zn:Zn}}^{\text{C14}} = 35000$	[19]
	$G_{\text{Mg:Mg,Zn}}^{\text{C14}} = G_{\text{Zn:Mg,Zn}}^{\text{C14}} = 8000$	[19]
	$G_{\text{Gd:Gd}}^{\text{C14}} - {}^0G_{\text{Gd}}^{\text{HCP\_A3}} = +5000$	This work
	$G_{\text{Gd:Mg}}^{\text{C14}} - 0.667{}^0G_{\text{Gd}}^{\text{HCP\_A3}} - 0.333{}^0G_{\text{Mg}}^{\text{HCP\_A3}} = +20000 - 3.324T$	This work
	$G_{\text{Mg:Gd}}^{\text{C14}} - 0.667{}^0G_{\text{Mg}}^{\text{HCP\_A3}} - 0.333{}^0G_{\text{Gd}}^{\text{HCP\_A3}} = -10000 + 3.324T$	This work
	$G_{\text{Mg,Zn}}^{\text{C14}} - 0.48{}^0G_{\text{Mg}}^{\text{HCP\_A3}} - 0.52{}^0G_{\text{Zn}}^{\text{HCP\_Zn}} = -9479.23 + 2.37T$	[19]
	$G_{\text{Mg,Zn}_3}^{\text{C14}} - 0.4{}^0G_{\text{Mg}}^{\text{HCP\_A3}} - 0.6{}^0G_{\text{Zn}}^{\text{HCP\_Zn}} = -10881.24 + 2.72T$	[19]
Mg <sub>7</sub> Zn <sub>3</sub> model: (Mg) <sub>0.7183</sub> (Zn) <sub>0.2817</sub>	$G_{\text{Mg:Zn}}^{\text{Mg}_7\text{Zn}_3} - 0.7183{}^0G_{\text{Mg}}^{\text{HCP\_A3}} - 0.2817{}^0G_{\text{Zn}}^{\text{HCP\_Zn}} = -4728.75 + 0.5T$	[19]
Mg <sub>2</sub> Zn <sub>11</sub> model: (Mg) <sub>0.1539</sub> (Zn) <sub>0.8461</sub>	$G_{\text{Mg:Zn}}^{\text{Mg}_2\text{Zn}_{11}} - 0.1539{}^0G_{\text{Mg}}^{\text{HCP\_A3}} - 0.8461{}^0G_{\text{Zn}}^{\text{HCP\_Zn}} = -5678.33 + 1.4196T$	[19]
Gd <sub>13</sub> Zn <sub>58</sub> model: (Gd) <sub>0.183</sub> (Zn) <sub>0.817</sub>	$G_{\text{Gd:Zn}}^{\text{Gd}_{13}\text{Zn}_{58}} - 0.183{}^0G_{\text{Gd}}^{\text{HCP\_A3}} - 0.817{}^0G_{\text{Zn}}^{\text{HCP\_Zn}} = -34222.2 + 1.8T$	This work
Gd <sub>2</sub> Zn <sub>17</sub> model: (Gd) <sub>0.105</sub> (Zn) <sub>0.895</sub>	$G_{\text{Gd:Zn}}^{\text{Gd}_2\text{Zn}_{17}} - 0.105{}^0G_{\text{Gd}}^{\text{HCP\_A3}} - 0.895{}^0G_{\text{Zn}}^{\text{HCP\_Zn}} = -26145.9 + 2.0T$	This work
Gd <sub>3</sub> Zn <sub>11</sub> model: (Gd) <sub>0.214</sub> (Zn) <sub>0.786</sub>	$G_{\text{Gd:Zn}}^{\text{Gd}_3\text{Zn}_{11}} - 0.214{}^0G_{\text{Gd}}^{\text{HCP\_A3}} - 0.786{}^0G_{\text{Zn}}^{\text{HCP\_Zn}} = -36530 + 1.8T$	This work
Gd <sub>3</sub> Zn <sub>22</sub> model: (Gd) <sub>0.12</sub> (Zn) <sub>0.88</sub>	$G_{\text{Gd:Zn}}^{\text{Gd}_3\text{Zn}_{22}} - 0.12{}^0G_{\text{Gd}}^{\text{HCP\_A3}} - 0.88{}^0G_{\text{Zn}}^{\text{HCP\_Zn}} = -27700 + 1.9T$	This work

**Table 3** continued

Phase	Thermodynamic parameters	Ref.
GdZn <sub>12</sub> model: (Gd) <sub>0.077</sub> (Zn) <sub>0.923</sub>	$G_{\text{Gd:Zn}}^{\text{GdZn}_{12}} - 0.077^0 G_{\text{Gd}}^{\text{HCP\_A3}} - 0.923^0 G_{\text{Zn}}^{\text{HCP\_Zn}} = -20345.1 + 2.0T$	This work
GdZn <sub>2</sub> model: (Gd) <sub>0.333</sub> (Zn) <sub>0.667</sub>	$G_{\text{Gd:Zn}}^{\text{GdZn}_2} - 0.333^0 G_{\text{Gd}}^{\text{HCP\_A3}} - 0.667^0 G_{\text{Zn}}^{\text{HCP\_Zn}} = -45378.3 + 3.0T$	This work
GdZn <sub>3</sub> model: (Gd) <sub>0.25</sub> (Zn) <sub>0.75</sub>	$G_{\text{Gd:Zn}}^{\text{GdZn}_3} - 0.25^0 G_{\text{Gd}}^{\text{HCP\_A3}} - 0.75^0 G_{\text{Zn}}^{\text{HCP\_A3}} = -39242.6 + 2.0T$	This work
X model: (Mg) <sub>0.86</sub> (Gd) <sub>0.08</sub> (Zn) <sub>0.06</sub>	$G_{\text{Mg:Gd:Zn}}^{\text{X}} - 0.86^0 G_{\text{Mg}}^{\text{HCP\_A3}} - 0.08^0 G_{\text{Gd}}^{\text{HCP\_A3}} - 0.06^0 G_{\text{Zn}}^{\text{HCP\_Zn}} = -9000 + 3.1T$	This work
W model: (Mg) <sub>0.2</sub> (Gd) <sub>0.2</sub> (Mg,Zn) <sub>0.6</sub>	$G_{\text{Mg:Gd:Zn}}^{\text{W}} - 0.8^0 G_{\text{Mg}}^{\text{HCP\_A3}} - 0.2^0 G_{\text{Gd}}^{\text{HCP\_A3}} = -8500 + 4.1T$	This work
	$G_{\text{Mg:Gd:Zn}}^{\text{W}} - 0.2^0 G_{\text{Mg}}^{\text{HCP\_A3}} - 0.2^0 G_{\text{Gd}}^{\text{HCP\_A3}} - 0.6^0 G_{\text{Zn}}^{\text{HCP\_Zn}} = -41000 + 9.9T$	This work
I model: (Mg) <sub>0.3</sub> (Gd) <sub>0.1</sub> (Mg,Zn) <sub>0.6</sub>	$G_{\text{Mg:Gd:Mg}}^{\text{I}} - 0.9^0 G_{\text{Mg}}^{\text{HCP\_A3}} - 0.1^0 G_{\text{Gd}}^{\text{HCP\_A3}} = -5000 + 3.8T$	This work
	$G_{\text{Mg:Gd:Zn}}^{\text{I}} - 0.3^0 G_{\text{Mg}}^{\text{HCP\_A3}} - 0.1^0 G_{\text{Gd}}^{\text{HCP\_A3}} - 0.6^0 G_{\text{Zn}}^{\text{HCP\_Zn}} = -31000 + 8.6T$	This work

**Fig. 6** Calculated Zn–Gd phase diagram using the present thermodynamic description compared with the experimental data [23]

projection of the liquidus surface of the Mg–Zn–Gd system according to the present thermodynamic description. The calculated temperatures of invariant reactions presented in Table 5.

As a validation for the obtained database, Scheil model was used to simulate the process of non-equilibrium solidification of the Mg–5 at.% Zn–0.5 at.% Gd alloy. The point on the liquidus surface refers to the composition of Mg–5 at.% Zn–0.5 at.% Gd, and the line presents the solidification path of this alloy simulated by Scheil model. The calculated solidification curve about temperature versus fraction of solid, shown in Fig. 9, is in accordance with the experimental results of Liu [38], in which W phase was observed within the lamellar I phase. Being in agreement with the thermodynamic prediction, W phase firstly

**Table 4** Invariant reactions in the Gd–Zn system

Reaction	$T$ (K)		Composition, $x_{\text{Zn}}^{\text{I}}$ (at.%)	
	Exp [26]	Cal	Exp [26]	Cal
BCC_A2 $\rightarrow$ L + HCP_A3	1473	1470	8	9.2
L $\rightarrow$ GdZn(BCC_B2)	1293	1300	–	–
L $\rightarrow$ GdZn <sub>2</sub>	1283	1281	–	–
L $\rightarrow$ GdZn(BCC_B2) + GdZn <sub>2</sub>	1218	1221	59	58.2
L $\rightarrow$ Gd <sub>2</sub> Zn <sub>17</sub>	1208	1205	–	–
L $\rightarrow$ Gd <sub>13</sub> Zn <sub>58</sub>	1193	1185	–	–
L + Gd <sub>2</sub> Zn <sub>17</sub> $\rightarrow$ Gd <sub>3</sub> Zn <sub>22</sub>	–	1182	–	85.3
L + GdZn <sub>2</sub> $\rightarrow$ GdZn <sub>3</sub>	1178	1175	–	98.0
L $\rightarrow$ Gd <sub>13</sub> Zn <sub>58</sub> + Gd <sub>3</sub> Zn <sub>22</sub>	1158	1168	–	–
L + Gd <sub>13</sub> Zn <sub>58</sub> $\rightarrow$ Gd <sub>3</sub> Zn <sub>11</sub>	–	1168	–	98.5
L $\rightarrow$ GdZn <sub>3</sub> + Gd <sub>3</sub> Zn <sub>11</sub>	–	1167	–	100
L $\rightarrow$ GdZn(BCC_B2) + HCP_A3	1053	1046	27	100
L + Gd <sub>2</sub> Zn <sub>17</sub> $\rightarrow$ GdZn <sub>12</sub>	933	936	98.5	28.8
L $\rightarrow$ GdZn <sub>12</sub> + HCP_Zn	692.5	693	–	99.9

appears during solidification, then I phase appears via L + W  $\rightarrow$  I + ( $\alpha$ Mg).

Overall, the results of the current database are considered fairly satisfactory. The resultant thermodynamic database can be applied to study various phase equilibrium-related materials problems.

## Conclusion

The partial isothermal section of Mg–Zn–Gd ternary system in Mg-rich corner at 673 K was investigated.

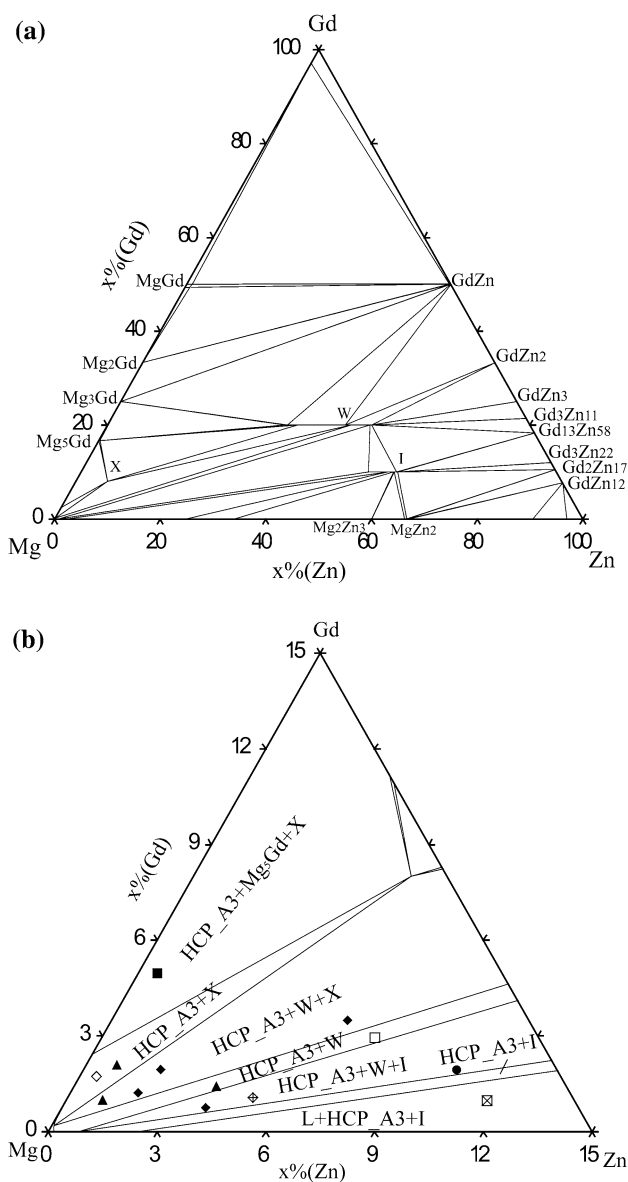


**Fig. 7** (a) Calculated phase diagram of Mg–Zn–Gd ternary system at 673 K. (b) Enlargement in the Mg-rich corner together with the experimental data

Three ternary phases, X-(Mg<sub>12</sub>ZnGd), W-(Mg<sub>3</sub>Zn<sub>3</sub>Gd<sub>2</sub>) and I-(Mg<sub>3</sub>Zn<sub>6</sub>Gd<sub>1</sub>), are identified and they are directly in equilibrium with the Mg solid solution. The Zn–Gd and Mg–Zn–Gd systems are thermodynamically modeled for the first time using the CALPHAD method. In particular, the order/disorder transition between BCC\_B2 and BCC\_A2 in these system has been taken into account. The calculated phase diagrams are in reasonable agreement with available experimental data. The resultant thermodynamic database is applied to case studies, showing that the present thermodynamic description of the Mg–Zn–Gd system is reliable for computer-assisted design of magnesium-based materials.

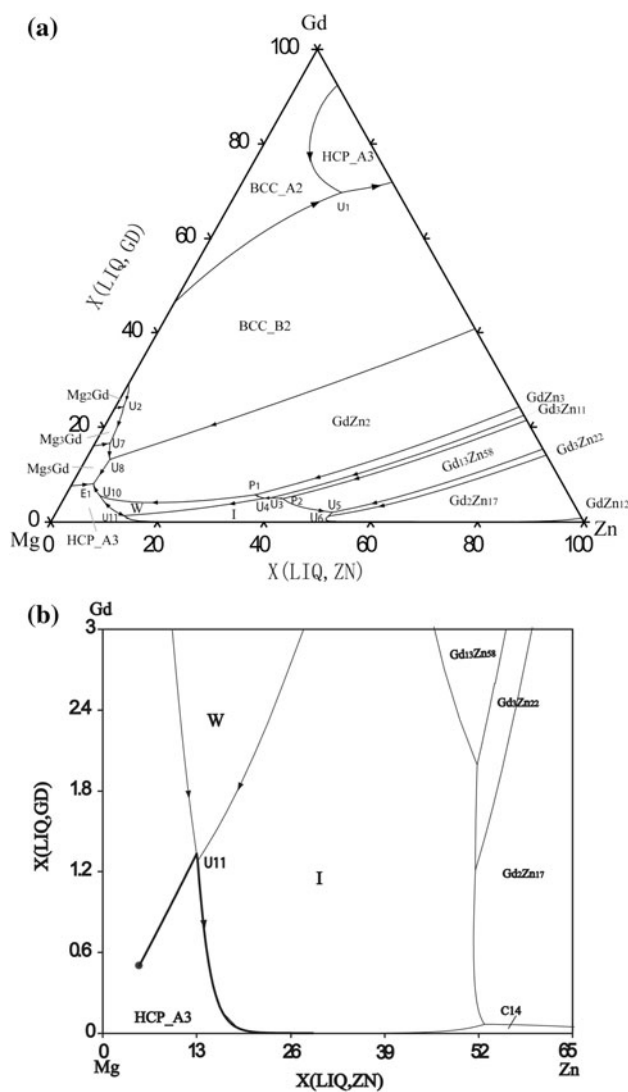


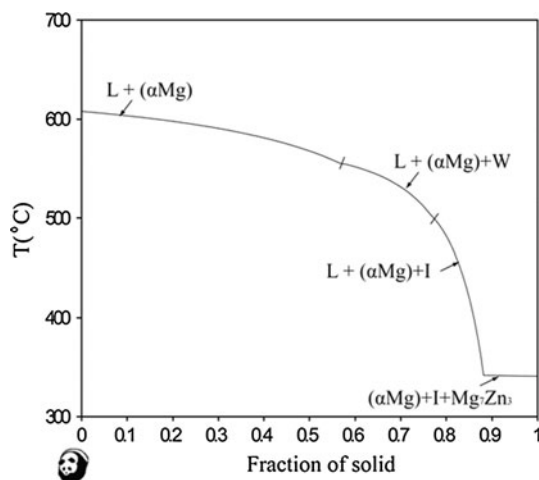
**Fig. 8** Calculated liquidus projection of Mg–Zn–Gd system using the present thermodynamic description (a) full view (b) in the Mg-rich corner. The point refers to the composition of Mg–5 at.% Zn–0.5 at.% Gd

**Table 5** Calculated invariant reactions in the Mg–Zn–Gd ternary system

Type	Reaction	Temperature (K)
Ternary quasi-peritectic		
U <sub>1</sub>	L + BCC_A2 → BCC_B2 + HCP_A3	1105.12
U <sub>2</sub>	L + Mg <sub>2</sub> Gd → BCC_B2 + Mg <sub>3</sub> Gd	983.55
U <sub>3</sub>	L + Gd <sub>3</sub> Zn <sub>11</sub> → I + GdZn <sub>3</sub>	967.29
U <sub>4</sub>	L + GdZn <sub>3</sub> → I + W	964.84
U <sub>5</sub>	L + Gd <sub>13</sub> Zn <sub>58</sub> → I + Gd <sub>3</sub> Zn <sub>22</sub>	939.60
U <sub>6</sub>	L + Gd <sub>3</sub> Zn <sub>22</sub> → I + Gd <sub>2</sub> Zn <sub>17</sub>	921.45
U <sub>7</sub>	L + Mg <sub>3</sub> Gd → Mg <sub>5</sub> Gd + BCC_B2	910.77
U <sub>8</sub>	L + BCC_B2 → GdZn <sub>2</sub> + Mg <sub>5</sub> Gd	879.29
U <sub>9</sub>	L + Gd <sub>2</sub> Zn <sub>17</sub> → I + C14	825.69
U <sub>10</sub>	L + W → GdZn <sub>2</sub> + HCP_A3	818.00

**Table 5** continued

Type	Reaction	Temperature (K)
U <sub>11</sub>	L + W → HCP_A3 + I	806.12
U <sub>12</sub>	L + Gd <sub>2</sub> Zn <sub>17</sub> → C14 + GdZn <sub>12</sub>	783.33
U <sub>13</sub>	L + C14 → I + Mg <sub>2</sub> Zn <sub>3</sub>	688.95
U <sub>14</sub>	L + C14 → GdZn <sub>12</sub> + Mg <sub>2</sub> Zn <sub>11</sub>	654.39
U <sub>15</sub>	L + Mg <sub>2</sub> Zn <sub>3</sub> → I + MgZn	620.15
U <sub>16</sub>	L + HCP_A3 → I + Mg <sub>7</sub> Zn <sub>3</sub>	614.17
Ternary peritectic		
P <sub>1</sub>	L + GdZn <sub>3</sub> + GdZn <sub>2</sub> → W	977.27
P <sub>2</sub>	L + Gd <sub>3</sub> Zn <sub>11</sub> + Gd <sub>13</sub> Zn <sub>58</sub> → I	970.16
Ternary eutectic		
E <sub>1</sub>	L → GdZn <sub>2</sub> + HCP_A3 + Mg <sub>5</sub> Gd	798.22
E <sub>2</sub>	L → GdZn <sub>12</sub> + Mg <sub>2</sub> Zn <sub>11</sub> + HCP_ZN	640.36
E <sub>3</sub>	L → I + MgZn + Mg <sub>7</sub> Zn <sub>3</sub>	614.14

**Fig. 9** Simulation of non-equilibrium solidification of Mg–5 at.% Zn–0.5 at.% Gd with Scheil model

**Acknowledgements** This work was financially supported by the National Science Foundation of China (Grant no. 50731002), Center of Phase Diagram & Materials Design and Manufacture Foundation (Grant no. 1773-206001146) and Excellent PhD Thesis Support Foundation of Central South University (Grant no. 2008yb013).

## References

- Mordike BL, Ebert T (2001) Mater Sci Eng A 302:37
- Schumann S, Friedrich H (2003) Mater Sci Forum 51:419
- Luo AA (2004) Int Mater Rev 49:13
- Nie JF, Muddle BC (2000) Acta Mater 48:1691
- Nayeb-Hashemi AA, Clark JB (1998) Phase diagrams of binary magnesium alloys. ASM International, Metals Park

- Nie JF, Gao X, Zhu SM (2003) Scr Mater 53:1049
- Avedesian MM, Baker H (1999) Magnesium and magnesium alloys. ASM International, Materials Park
- Abe E, Sato TJ, Tsai AP (2000) Mater Sci Eng A 294–296:29
- Uhrig E, Brühne S, Assmus W, Grüner D, Kreiner G (2005) J Cryst Growth 275:e1987
- Liu Y, Yuan GY, Lu C, Ding WJ (2006) Scr Mater 55:919
- Liu Y, Yuan GY, Lu C, Ding WJ, Jiang JZ (2008) J Mater Sci 43:5527. doi:10.1007/s10853-008-2839-z
- Janot C (1994) Quasicrystals. Clarendon Press, Oxford
- Yamasaki M, Sasaki M, Nishijima M et al (2007) Acta Mater 55:6798
- Wu YJ, Lin DL, Zeng XQ, Peng LM, Ding WJ (2009) J Mater Sci 44:1607. doi:10.1007/s10853-008-3213-x
- Wu YJ, Peng LM, Zeng XQ, Lin DL, Ding WJ (2010) Mater Sci Forum 654–656:623
- Zhang S, Yuan GY, Lu C, Ding WJ (2011) J Alloys Compd 509:3515
- Kaufman L, Bernstein H (1970) Computer calculation of phase diagrams. Academic Press, New York
- Agarwal R, Fries SG, Lukas HL, Petzow G, Sommer F, Chart TG, Effenberg G (1992) Z Metallkd 83:216
- Liang P, Tarfa T, Robinson JA, Wagner S, Ochin P, Harmelin MG et al (1998) Thermochim Acta 314:87
- Berche A, Drescher C, Rogez J, Record MC, Brühne S, Assmus W (2010) J Alloys Compd 503:44
- Cacciamani G, Saccone A, Borzone G, Delfino S, Ferro R (1992) Thermochim Acta 199:17
- Cacciamani G, De Negri S, Saccone A, Ferro R (2003) Intermetallics 11:1135
- Guo C, Du Z, Li C (2007) Calphad 31:75
- Massalski TB, Okamoto H, Subramanian PR, Kacprzak L (1990) Binary alloy phase diagrams, 2nd edn. ASM International, Materials Park
- Bruzzone G, Fornasini ML, Merlo F (1970) J Less Common Met 22:253
- Sccone A, Cardinale AM, Delfino S, Ferro R (2001) Z Metallkd 92:959
- Chiotti P, Mason JT (1973) Metall Trans 4:1527
- Borzone G, Cacciamani G, Ferro R, Charles J, Hertz J (1987) J Less Common Met 128:297
- Padezhnova EM, Mel'nik EV, Miliyevskiy RA, Dobatkina TV, Kinzhbalo VV (1982) Russ Metall 4:185
- SGTE (2008) SGTE Pure Elements (Unary) Database (version v 4.6), developed by SGTE (Scientific Group Thermodata Europe), 1991–2008, and provided by TCSAB. SGTE website, <http://www.sgte.org>
- Redlich O, Kister AT (1948) Ind Eng Chem 40:345
- Ansara I, Dupin N, Lukas HL, Sundman B (1997) J Alloys Compd 247:20
- Dupin N, Ansara I (1999) Z Metallkd 90:76
- Sundman B, Agren J (1981) J Phys Chem Solids 42:297
- Toffolon C, Servant C, Gachon JC, Sundman B (2002) J Phase Equilib 23:134
- Anderson JO, Helander T, Hoglund L, Shi P, Sundman B (2002) CALPHAD 26:273
- PANDAT Software, CompuTherm, LLC, Madison, WI, USA. <http://www.compuTherm.com>
- Liu Y (2007) Ph.D. thesis, Shanghai Jiao Tong University